IRRADIATION TEST OF MOX FUEL IN THE HALDEN REACTOR AND THE ANALYSIS OF MEASURED DATA WITH THE FUEL PERFORMANCE CODE COSMOS

WOLFGANG WIESENACK[1], BYUNG-HO LEE[2] and DONG-SEONG SOHN[2*]
[1]OECD Halden Reactor Project (Institutt for energiteknikk)
P.O. Box 173, N-1751 Halden, Norway
[2]Korea Atomic Energy Research Institute
150 Deokjin-dong, Yuseong, Daejeon 305-353, Korea
*Corresponding author. E-mail : dssohn@kaeri.re.kr

Received July 30, 2005

The burning-out of excess plutonium from the reprocessing of spent nuclear fuel and from the dismantlement of nuclear weapons is recently emphasized due to the difficulties in securing the final repository for the spent fuel and the necessity to consume the ex-weapons plutonium. An irradiation test in the Halden reactor was launched by the OECD Halden Reactor Project (HRP) to investigate the in-pile behavior of plutonium-embedded fuel as a form of mixed oxide (MOX) and of inert matrix fuel (IMF). The first cycle of irradiation was successfully accomplished with good integrity of test fuel rods and without any undesirable fault of instrumentations. The test results revealed that the MOX fuel is more stable under irradiation environments than IMF. In addition, MOX fuel shows lower thermal resistance due to its better thermal conductivity than IMF. The on-line measured in-pile performance data of attrition milled MOX fuel are used in the analysis of the in-pile performance of the fuel with the fuel performance code, COSMOS. The COSMOS code has been developed for the analysis of MOX fuel as well as UO_2 fuel up to high burnup and showed good capability to analyze the in-reactor behavior of MOX fuel even with different instrumentation.

KEYWORDS : Halden Reactor Project, In-pile Test, Instrumentation, MOX Fuel, Fuel Performance Code, Densification

1. INTRODUCTION

One of the options to consume the excess plutonium can be the incorporation of the plutonium into MOX fuel or IMF (Inert Matrix Fuel). Recently, this option is more emphasized due to the difficulties in securing the permanent repository for the spent fuel.

An in-pile irradiation test of MOX and IMF fuel was initiated in the Halden reactor, as IFA 651 experiment, to compare the in-reactor performance under irradiation condition similar to those in LWR's. Of particular interest are fuel thermal conductivity and its degradation with burnup, fission gas release, fuel densification, and fuel swelling which can all be derived from the in-core performance data obtained from the instrumentation. The experiment is executed within the Joint Programme of the Halden Reactor Project, but is sponsored by the Korean Atomic Energy Research Institute (KAERI), British Nuclear Fuels plc (BNFL) and the Swiss Paul Scherrer Institut (PSI).

The in-pile performance data obtained from attrition milled MOX fuel was compared with the prediction of the fuel performance analysis code COSMOS [1].

The following instrumentation can be utilized for both fresh and pre-irradiated fuels irradiation in the Halden reactor:

(1) Fuel thermocouples or expansion thermometers, which measure the fuel centre temperature;
(2) Bellows pressure transducers, providing data on fission gas release by measuring the rod inner pressure;
(3) Fuel stack elongation detectors, with which densification and swelling behavior can be assessed;
(4) Cladding elongation detectors, providing data on the onset and the amount of pellet - clad interaction, permanent deformation as well as relaxation of fuel and cladding as function of power and burn-up;

In the present paper, the in-pile data obtained from the primary instrumentation during the first irradiation cycle are described and analyzed. And then, the comparison of the COSMOS code prediction with the attrition milled MOX fuel data is described with brief introduction of the code.

2. DESCRIPTION OF IRRADIATION TEST, IFA-651

2.1 Description of Rig

Fig. 1 shows the schematics of the rig, IFA-651. The rig holds three IMF rods and three MOX rods in one cluster. Two IMF rods and two MOX rods contain fuel manufactured at PSI using an attrition milling process (ATT) developed at KAERI [2]. For comparison purposes, the remaining IMF rod and MOX rod contain PSI fuel manufactured using a wet co-precipitation process (CO) and BNFL fuel manufactured using the short binderless route (SBR) [3], respectively.

To measure the fuel temperature, four rods have a thermocouple at the top end, while the remaining two rods are equipped with expansion thermometers. All rods have pressure transducers at the bottom end. In addition, three rods (two IMF and one MOX) are instrumented with stack elongation detectors at the top of the fuel stack. An accurate determination of the power distribution is achieved with three co-linear neutron detectors at three different elevations and three axi-symmetric neutron detectors at half height of the fuel stack. The main rod fabrication data are compiled in Table 1.

2.2 Power and Burnup Determination

The accurate power determination is the prerequisite for a successful in-pile test. The rig power can be directly measured by calorimetric means in subcooled flow condi-

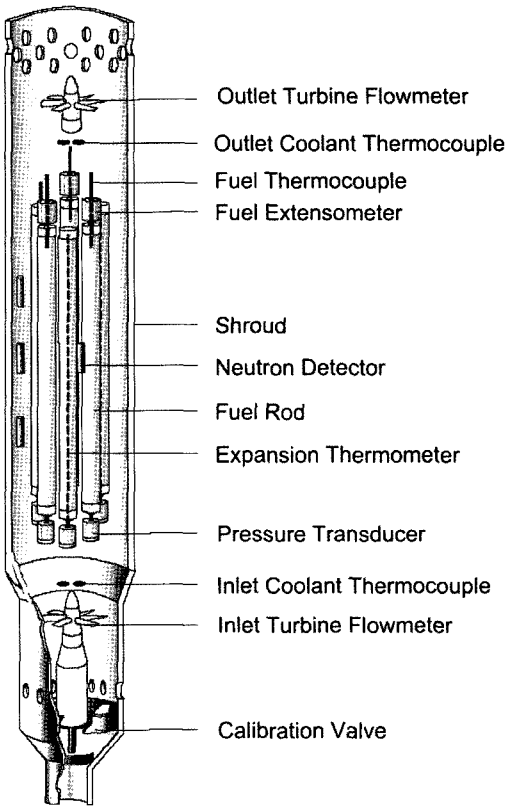

Fig. 1. Schematic of the Irradiation Test Rig

Table 1. Main Fabrication Data of the IMF/MOX Fuel Study IFA-651

Rod Number	1	2	3	4	5	6
FUEL PELLETS						
Fuel type	MOX-SBR	IMF-ATT	MOX-ATT	IMF-CO	IMF-ATT	MOX-ATT
Fissile Pu, wt%metal	5.98	14.2	5.85	13.6	14.2	5.85
Density, g/cm^3	10.401	6.294	10.404	5.833	6.298	10.434
Density, %TD	94.6	95.5	94.6	88.4	95.5	94.9
Outer diameter, mm	8.200	8.192	8.191	8.195	8.191	8.192
Hollow pellet ID, mm	1.8	1.8	2.0	1.8	2.0	1.8
CLADDING						
Material	Low tin Zircaloy-4, outer diameter 9.50 mm					
Inner diameter, mm	8.358	8.360	8.349	8.361	8.364	8.354
FUEL ROD						
Fill gas & pressure	Helium, 10 bar					
Free volume, cc	8.4	9.4	8.3	10.4	8.4	8.5
Instrumentation	TF,PF	TF,PF,EF	ET,PF	TF,PF,EF	ET,PF	TF,PF,EF

tions whereas the rod power is obtained by multiplying a power conversion factor (PCF) for each rod with neutron detector signal and a depletion function. The two-dimensional transport code, HELIOS, is used to determine the relative contribution of each fuel rod to the total rig power.

The first rig power calibration was performed at the beginning of the irradiation of IFA-651. In total four rig power measurements were performed to obtain the ratio (KG factor, kW/nA) of the rig power to the average neutron signal. The mean KG factor of 0.750 kW/nA was obtained with a maximum difference of only 2.6%. The HELIOS-estimated ratio of 0.774 kW/nA is only 3% greater than the experimental value, which confirms that HELIOS accurately models the rig-wide characteristics and that the HELIOS predictions can be applied for proper power determination. The PCF factors were adjusted by 3% from their HELIOS predicted values so that the values used are in accordance with the definitive KG factor of 0.750 kW/nA which was obtained experimentally.

The second rig power calibration was performed at the end of the first cycle to determine the accuracy of the depletion functions calculated by HELIOS. A mean value of 0.701 kW/nA was obtained with a difference of only 0.7% between the two rig power measurements performed at this time. From the comparison of the first and second power calibration, the measured rig average depletion value is 0.935 at the time of the second power calibration. The HELIOS predicted a value of 0.942 which differs only 0.7% from the measured rig average depletion value. The depletion functions are therefore judged to be sufficiently accurate.

3. IN-PILE BEHAVIOR OF IFA-651

The following sections give an overview of the data obtained from the primary instrumentation for assessment of fuel behavior. With the on-line measured in-pile data, some basic conclusions regarding performance can also be drawn.

3.1 Fuel Temperatures

The upper part of Fig. 2 shows the power history of the test fuel for the first weeks of operation. After calibration, four power up-ramps were carried out which are marked in the figure. The measured temperatures of rod 5 (IMF-attrition milled) and rod 6 (MOX-attrition milled) are plotted in the lower part of Fig. 2 against linear heat rating for the four ramps. Several features can be noted.

Firstly, a distinct difference is apparent between the temperatures of the MOX fuel and the IMF fuel. This reflects the differences in thermal conductivity, i.e. the IMF fuel has about 35% lower conductivity than MOX fuel (which, in turn, has about 8% lower conductivity than urania fuel).

Secondly, a change of the temperature – power relation

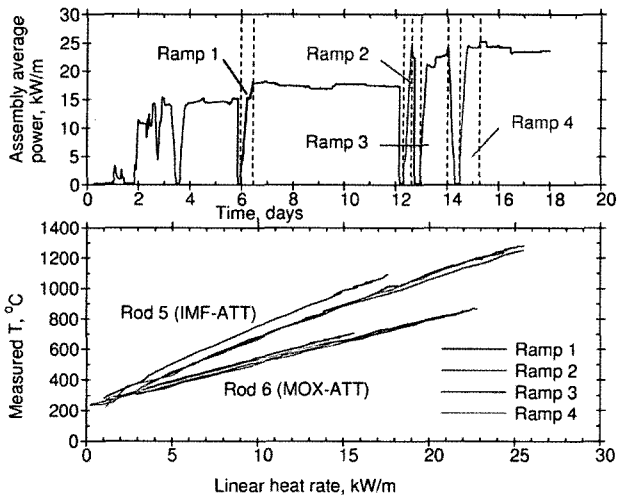

Fig. 2. Initial Power History and Measured Fuel Temperatures of the First four Power Ramps

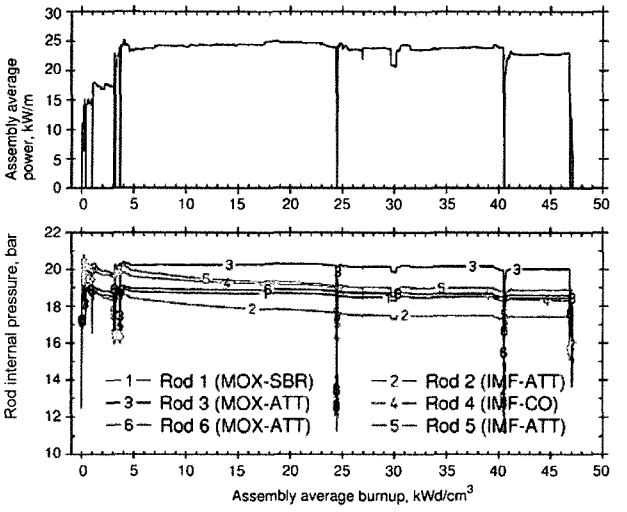

Fig. 3. Development of the Rod Internal Pressure During the First Irradiation Cycle in the Halden Reactor

can be noted between the first and second power ramp. This is due to reorganization of the fuel configuration, i.e. radial cracking and subsequent relocation causing a reduction of the fuel-clad gap and lower fuel temperatures as a consequence. The change is more pronounced for the IMF fuel.

3.2 Rod Pressure

The rods were initially filled with helium at 10 bar at room temperature. The measured pressures for all rods

are plotted in Fig. 3, together with the assembly average linear heat rate. The pressure of the IMF rods (2, 4, 5) decreases with burnup. The IMF rods 2 and 5 manufactured by the same process (attrition milling) show almost the same pressure decreases. The IMF rod 4 manufactured by co-precipitation indicates a slightly lower decrease in pressure. The pressure of the MOX rods 1, 3 and 6 (both SBR and ATT) initially dropped slightly (by ~ 0.5 bar), then rapidly stabilized.

At this low level of exposure and at the low fuel temperatures, fission gas release should not occur (the fission gas release behavior of IMF fuel under irradiation conditions was actually not known before this experiment was executed). The pressure changes are therefore only due to volume changes because of fuel densification and swelling. The MOX fuels exhibit better stability as derived from the pressure data.

3.3 Fuel Stack Length Changes

Fuel stack elongation data can be used to infer densification and swelling. In IFA-651, rods 2, 4 and 6 are equipped with stack elongation detectors.

The data obtained during the first irradiation cycle are shown in Fig. 4. Again, a marked difference between the MOX and IMF types of fuel can be noted. The elongation data (the marks at shut-downs designate values at hot stand-by conditions) indicate that the stack lengths of the IMF rods undergo a permanent reduction of about 6 mm by the end of cycle, whereas the MOX stack length has decreased by only about 1 mm at the same time.

The end-of-cycle burnup of 47 kWd/cm^3 corresponds to about 4.5 MWd/kg for standard fuels (MOX, UO_2). At such an exposure, densification is mostly complete, and this appears to be the case for the MOX fuel (rod 6) and the attrition milled IMF fuel (rod 2), while the co-precipitated IMF fuel (rod 4) seems to continue this process.

The experiment will continue in the Halden Reactor until a burnup equivalent to about 40 MWd/kg (IMF) and 50 MWd/kg (MOX) is reached by the end of 2006 and 2007, respectively.

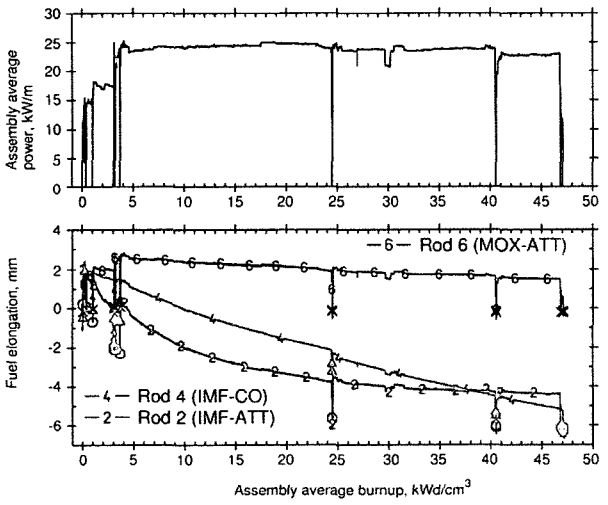

Fig. 4. Fuel Stack Elongation During the First Irradiation Cycle

4. COMPARISION OF THE IN-PILE TEST RESULTS WITH COSMOS CODE PREDICTION

The in-pile performance of the test fuels was monitored through instrumentation providing the on-line measured in-pile data. The fuel performance analysis code COSMOS was used to compare the measured performance data of attrition milled MOX fuel with code prediction. LWR MOX fuel is different from typical UO_2 fuel in that it contains up to about 10 wt% of Pu from the beginning. Due to difference in microstructure arising from the addition of Pu, the following features should be considered when analyzing MOX fuel with performance models for UO_2 fuel: 1) change in thermo-mechanical properties such as thermal conductivity and thermal expansion coefficient, 2) change in radial power depression in a fuel rod as a function of Pu fissile content, 3) change in the mechanism of fission gas release resulting from heterogeneous microstructure of MOX fuel depending on the manufacturing method, and 4) high burnup phenomena of fuel such as rim formation and thermal conductivity degradation. The mechanistic thermal conductivity and fission gas release models implemented in COSMOS code are described below.

4.1 Brief Description of the COSMOS Code

4.1.1 Thermal Conductivity Model

In the COSMOS code, the general thermal conductivity applicable for two-phase material [4] is used to assess the thermal conductivity of the MOX fuel containing heterogeneity. The thermal conductivity of the MOX fuel can be estimated from a combination of the thermal conductivities for the matrix and Pu-rich agglomerates [5]:

$$k_{MOX} = k_{matrix} \cdot \left\{ 1 - a \cdot P_{PuR}^{\frac{2}{3}} \cdot \left[1 - \frac{1}{1 + \frac{1}{a} \cdot P_{PuR}^{\frac{1}{3}} \cdot \left(\frac{k_{matrix}}{k_{PuR}} - 1 \right)} \right] \right\}$$

where

k_{MOX} = integral thermal conductivity of MOX fuel,

k_{matrix} = thermal conductivity of a matrix in which a little fraction of Pu is included $= \frac{1}{A_{matrix} + B_{matrix} \cdot T}$

k_{PuR} = thermal conductivity of Pu-rich particles (W/m-K)

P_{PuR} = volumetric fraction of Pu-rich particles

a = anisotropy factor (a=1 means isotropic pore distribution).

The thermal conductivity of the matrix is derived from the Halden's model [6] with some relevant information on the MOX fuel. Considering the increment induced by the plutonium embedded into the matrix, the phonon-impurity term in k_{matrix} can be given by the expression

$$A_{matrix} = 0.1149 + 0.0035 \cdot BU + \Delta A_{MOX}$$

where ΔA_{MOX} is the increment of a constant A following the plutonium in the matrix of the MOX fuel. An increment of A, ΔA_{MOX} is assumed to be proportional to the plutonium content:

$$\Delta A_{MOX} = \beta \cdot q$$

The quantity of q is determined from the fraction of plutonium distributed in the matrix not in the Pu-rich agglomerates. The newly suggested Pu addition factor would be expected to cover the thermal conductivity reduction through a possible modification of the stoichiometry in the range, 1.990 to 1.995 as soon as irradiation starts [7]. The lattice resistivity theory suggests a phonon-phonon term of

$$B_{matrix} = \left(2.475 \times 10^{-4} - 7.291 \times 10^{-7} \cdot BU\right) \cdot \Delta B_{MOX}$$

where ΔB_{MOX} indicates the increment due to the plutonium distributed in the matrix and is given by

$$\Delta B_{MOX} = \left(\frac{W_{MOX}(q)}{W_{UO_2}}\right)\left(\frac{a_{0,MOX}(q)}{a_{0,UO_2}}\right)\left(\frac{T_{m,UO_2}(BU)}{T_{m,MOX}(q,BU)}\right)$$

where W_j, $a_{0,j}$, and $T_{m,j}$ are the molecular weight, lattice parameter and melting temperature of j (MOX or UO_2), respectively.

The local thermal conductivity for Pu-rich particles is estimated by Phillipponeau's model [8].

Fig. 5(a) shows the ratio of the homogeneous MOX to UO_2 thermal conductivity for the plutonium contents of ~7% which is a typical content in LWR MOX fuel. The ratio of the thermal conductivity of MOX to UO_2 fuel increases with the temperature, whereas the burnup makes the thermal conductivity increase significantly, especially in the lower temperature region. The thermal conductivity of MOX fuel ranges from 85 to 92% of UO_2 at the beginning-of-its-life.

Since little relevant data on Pu-rich particles is available, results of an international MOX program [9] and Siemens-KWU [10] are used to characterize the inhomogeneous MOX microstructure of the un-irradiated and irradiated fuel. The ratio of the thermal conductivity of the inhomogeneous MOX to UO_2 is plotted in Fig. 5(b) as a function of burnup and temperature. The newly proposed model indicates a reduction in the MOX thermal conductivity

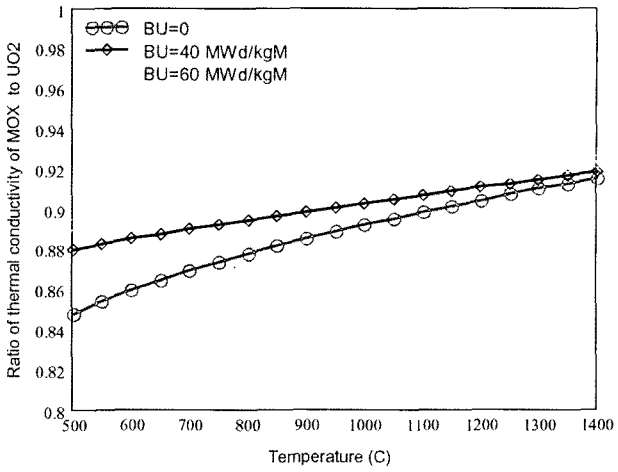

Fig. 5. Ratio of the MOX to UO_2 Thermal Conductivity for (a) Homogeneous and (b) Inhomogeneous MOX as a Function of the Temperature

ranging from 4 to 8 % when compared to UO_2 fuel at the beginning of its life.

For both the homogeneous and inhomogeneous MOX fuel, the difference between the MOX and UO_2 thermal conductivity decreases with the temperature because the electronic conduction becomes increasingly important at higher temperatures.

It should be noted that the burnup effect on the thermal conductivity is more significant in the inhomogeneous MOX than in the homogenous MOX fuel. This is caused by assuming that the burnup is three times as high in the Pu-rich agglomerates as in the matrix. If the burnup in the agglomerate is lower, the burnup effect in the inhomogeneous MOX fuel would be reduced.

This reduction is comparable to ENIGMA's [11] and Siemen's [12] MOX thermal conductivities, which are 8% less than that of standard UO_2 fuel and a relative decrease

of 4~5 %, respectively. However, it is slightly more conservative than BN's results [13] which show a 4% reduction of thermal conductivity for 10% Pu/(Pu+U) fuel. The present characteristics are adequate for the MOX fuel for a verification of the developed model although they are not sufficient to accommodate all the features of MOX fuel.

4.1.2 Fission Gas Release Model

Depending on the manufacturing method, heterogeneity can exist in the microstructure of MOX fuel pellets due to incomplete mixing of PuO_2 powder with UO_2 powder. There is some controversy over whether or not fission gas release is enhanced in MOX fuel compared with UO_2 fuel under similar operating conditions. Recent experiments showed that there seems to be little effect of microstructure in currently produced fuel. In addition, high gas release in MOX fuel is being attributed to higher operating powers in MOX fuel later in its life because the reactivity of MOX fuel falls more slowly with burnup than UO_2 fuel. However, it is necessary to have the ability to model the effect of heterogeneity to analyze the MOX fuel.

To analyze the effect of microscopic heterogeneity on fission gas release, a spherical model has been developed using the assumption that Pu-rich particles are distributed uniformly in the UO_2 matrix [14]. The fuel pellet is assumed to consist of equivalent spherical particles with diameter $D_{eq} = D_{agg} + 2\,L_{rec}$ surrounded by the UO_2 matrix containing a Pu-rich particle, where L_{rec} is the recoil length of fission products (see Fig. 6). The recoil length is assumed to be 6 μm. The diameter of an equivalent cell is then defined as follows:

$$D_{cell} = D_{agg} \Big/ \sqrt[3]{\frac{e_p - e_m}{e_a - e_m}}$$

where e_p is the average Pu content of the pellet, e_a is the Pu content of the Pu-rich particle, e_m is the Pu-content in the UO_2 matrix, D_{agg} is the average size of the Pu-rich particle.

The fission rates in the equivalent cell and matrix are calculated considering the effective enrichments in each zone. If the fuel parameters are such that D_{eq} is larger than D_{cell}, the fuel can be considered to be a homogeneous one.

The equivalent Pu content of the cell is calculated as follows:

$$e_{eq} = e_m + \left(\frac{D_{agg}}{D_{eq}}\right)^3 \cdot (e_a - e_m)$$

Fission rates in the equivalent cell and UO_2 matrix are given below, where the average fission rate Fav can be obtained from the average power density:

$$F_{eq} = \left(\frac{e_{eq}}{e_p}\right) \cdot F_{av} \quad \text{and} \quad F_m = \left(\frac{e_m}{e_p}\right) \cdot F_{av}$$

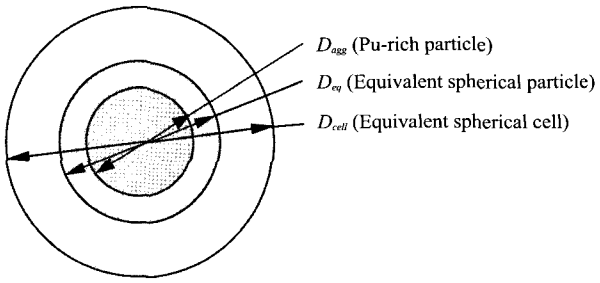

Fig. 6. An Equivalent Spherical Cell for a Pu-rich Particle

The average fission rates in each region are incorporated into the fission gas release model for UO_2 fuel, and are used to calculate the gas release in their respective regions.

4.1.3 Other COSMOS Features

With focusing on thermal conductivity and fission gas release in MOX fuel, the other characteristics of the COSMOS are as follows:

(1) Based on the measured rim characteristics of high burnup UO_2 fuel, the pressure of rim pores and additional pellet swelling due to rim formation have been modeled as a function of temperature, pellet average burnup and pore radius.

(2) Cladding oxidation [15] and creep modeling [16] are improved to take into account the void effect combined with water chemistry and heat treatment for cladding fabrication in high burnup fuels, respectively.

(3) Another important feature of the COSMOS code is that it can analyze fuel segments re-fabricated from base-irradiated fuel rods. This makes it possible to utilize a database obtained from international projects such as HRP and RISØ, many of which were collected from re-fabricated fuel segments. In particular, the COSMOS code has been improved to simulate the hole for a thermocouple to estimate the fuel centerline temperature of MOX fuel rods equipped with a thermocouple.

4.2 Comparison of the In-pile Test Data of IFA-651 with COSMOS Code Prediction

The first cycle irradiation of IFA-651 was successfully accomplished with good integrity of test fuel rods and without any undesirable fault of instrumentations. The in-pile test results of attrition milled MOX fuel in IFA-651 were rigorously analyzed and compared with the COSMOS code prediction. This comparison was mainly focused on the thermal analysis since the fuel temperature was below the threshold temperature for fission gas release during the first cycle irradiation.

The fuel and cladding geometry and all the other characteristics data were prepared according to the fabrication data. The coolant conditions were given based on the results

of on-line measurements. The rod wise axial power distribution data was provided for three axial nodes which were assessed using the signals from the self-powered neutron detectors. As described before, the neutron detectors are located at three different axial locations and at the center location there are three detectors arranged at three different angles in the rig.

In the comparison of the predicted and measured fuel temperature, rod average power was used in the calculation of the fuel temperature of Rod 3 (MOX-ATT). Rod 3 is equipped with an expansion thermometer measuring the average fuel temperature. On the other hand, the local power of the top node was used to calculate the fuel temperature at the thermocouple location in Rod 6 (MOX-ATT). The top node power was obtained by weighted interpolation of the three nodes power distribution.

Meaningful performance calculations requires that special attention should be paid the following four performance aspects: thermal conductivity, relocation, densification and swelling, and the radial power distribution. For the thermal conductivity, the model described in section 4.1.1 was used. The relocation parameters were determined from the data obtained from relevant MOX test series performed in the Halden reactor. The densification parameters were determined from rod internal pressure measurement data which reflect the internal volume change of the fuel rod.

Radial power distribution data was obtained from the nuclear physical calculation taking into account the Halden reactor conditions. The radial power depression in a MOX pellet is different from that of a conventional LWR UO_2 fuel due to the softer neutron spectrum in the core and the higher total Pu content in the fuel. Furthermore, two more features of the Halden reactor influence the radial power depression in the MOX fuel.

(1) Heavy water is used as moderator in the Halden reactor instead of the light water in the LWR which results in a different neutron spectrum in the Halden reactor due to the lower moderating power and higher moderating ratio of heavy water compared with those of light water.
(2) The fuel-to-moderator ratio of the Halden reactor, which also determines the degree of moderation of the fission neutrons, is different from that of a typical LWR.

Therefore, the neutron physics calculation for the radial depression should be made for the MOX fuel rods in the Halden reactor with due considerations for these factors.

In general, a function describing the radial power distribution is derived as a function of the enrichment (or Pu fissile content in case of MOX fuel), burnup and relative pellet radius based on the results of the nuclear physics calculations. For the present work, the HELIOS code is used to produce the reference radial power distribution using the conditions of the IFA-651 in the Halden reactor.

In an LWR pellet, the power density in the pellet periphery increases with burnup due to Pu-239 formation through absorption of epithermal neutrons by U-238 while

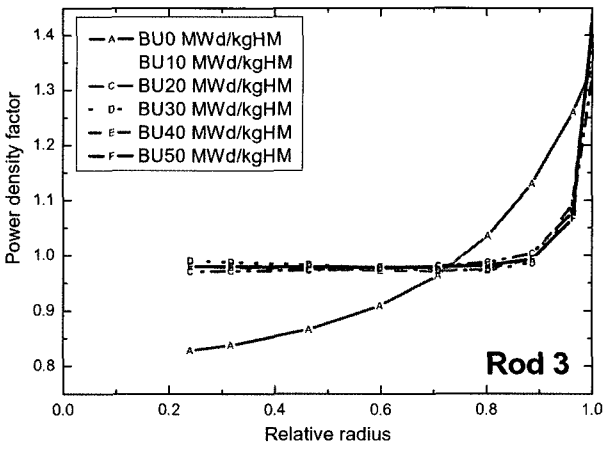

Fig. 7. Fitted Radial Power Distribution in (a) Rod 3 and (b) Rod 6

it shows the opposite trend in the pellet center region. In contrast, the power density in the MOX pellet for the Haden reactor as seen in Fig. 7 decreases with the burnup in the pellet outer area while it increases with the burnup in the central part of the pellet.

Carefully considering the input and model parameters discussed above, the thermal analysis was performed for both Rod 3, in which all the pellets have with a central hole for the expansion thermometer, and Rod 6, in which only the upper pellets are with a central hole to insert the thermocouple. Rod 3 is instrumented with an extension thermometer which measures the average fuel temperature of the fuel rod. Rod 6 has a thermocouple which is inserted from the top end of the fuel and thus measures local fuel center temperature. The linear power during power upramps was corrected for the delay of the neutron detector signal which is caused by the beta emission from activated vanadium after some minutes delay.

The variation of fuel temperature during power-up ramps throughout the first cycle was analyzed in order to check whether the input and modeling parameters are

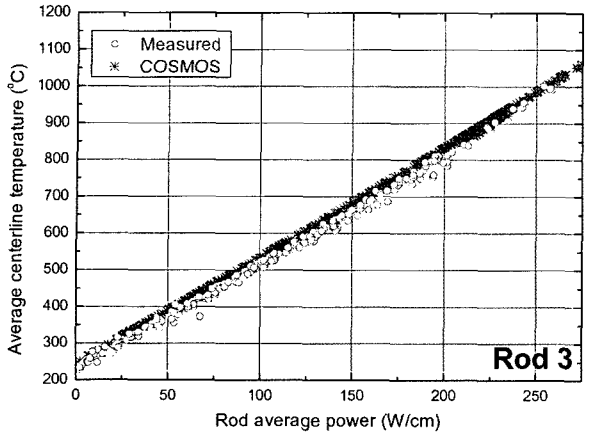

(a)

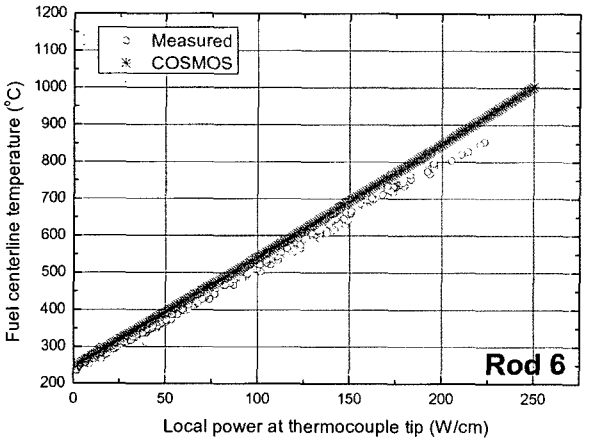

(b)

Fig. 8. Comparison of the COSMOS Calculated with Measured Centerline Temperature During Power-up Ramp for (a) Rod 3 (expansion thermometer) and (b) Rod 6 (thermocouple)

properly prepared. The expected fuel temperature was calculated at different power levels during a transient at the end of the first irradiation cycle. Fig. 8 shows the measured and calculated fuel temperature increase as a function of linear power for several ramps. Fig. 8 (a) shows the fuel average temperature against the fuel average linear power. Fig. 8 (b) displays the fuel temperature measure at the thermocouple tip as a function of the local linear power at the thermocouple position. It can be seen that the fuel temperatures in both Rod 3 and Rod 6 increases very linearly with linear heating rate and the measured data agrees well with the code prediction. The data measured from Rod 6 during the ramp at the early beginning of irradiation showed slight deviation from linearity at a heating rate of ~125 W/cm (see Fig. 9) while the measured results during other ramps showed good linearity and agreement with the code prediction.

An explanation for the nonlinear fuel temperature response may be stochastic fuel relocation. Rod 6 may have experienced such a prompt stochastic relocation process

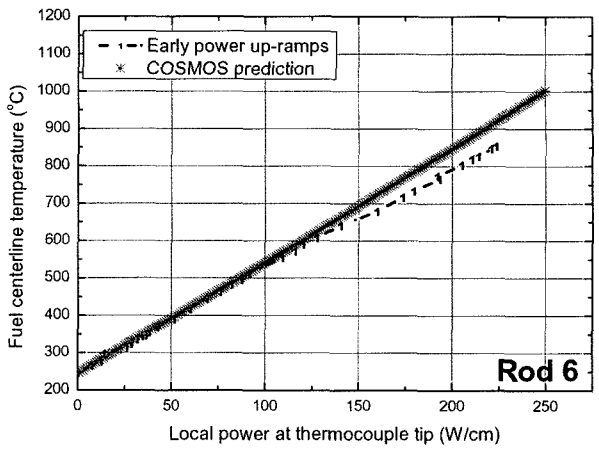

Fig. 9 . Comparison of the COSMOS Calculated with Measured Centerline Temperature During Power-up Ramp Performed at the Early Irradiation for Rod 6 (thermocouple)

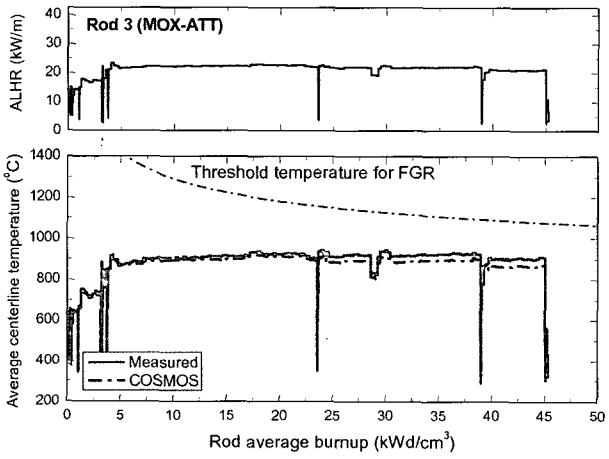

(a)

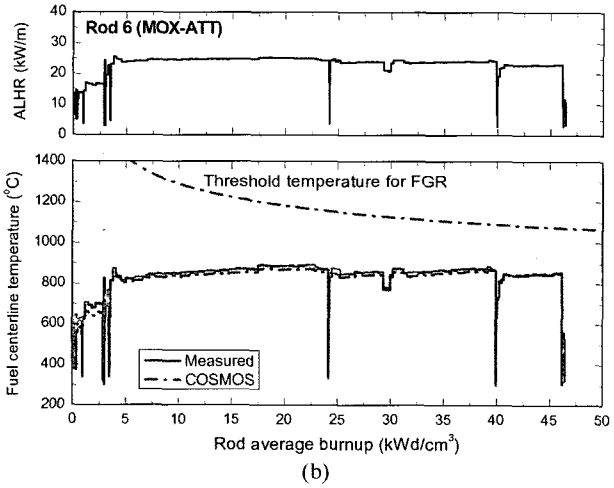

(b)

Fig. 10 . Comparison of the COSMOS Calculated Centerline Temperature with the Measured Value for (a) Rod 3 and (b) Rod 6

during the power increase at the early beginning of irradiation, and therefore the fuel temperature increase was diminished during the early power up-ramp due to the reduced gap by the relocation. On the other hand, it seems that the relocation in Rod 3 occurred more gradually and spread out during the irradiation period. Relocation may occur pellet-wise under certain local irradiation condition and thus the local temperature may be affected instantaneously by the relocation while the fuel average temperature may be affected gradually by the relocations at different positions at different time.

Before analyzing the steady state fuel temperature, the saturated densification values of the two fuel rods were estimated from the fuel volume changes which were calculated from the normalized rod internal pressure variation during the first cycle. The estimated maximum densification values were about 1% for Rod 3 and about 2% for Rod 6.

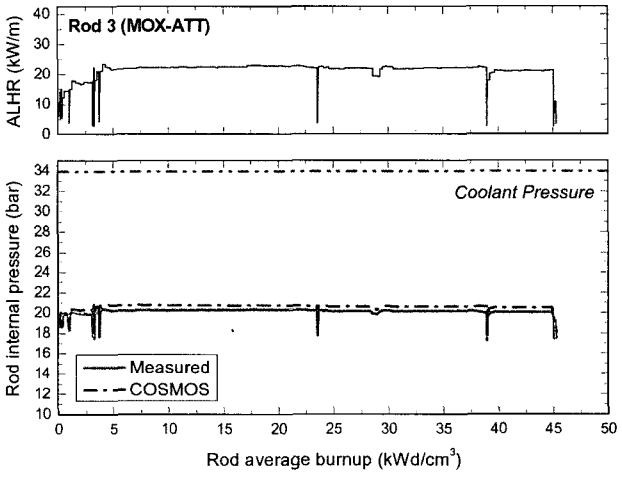

(a)

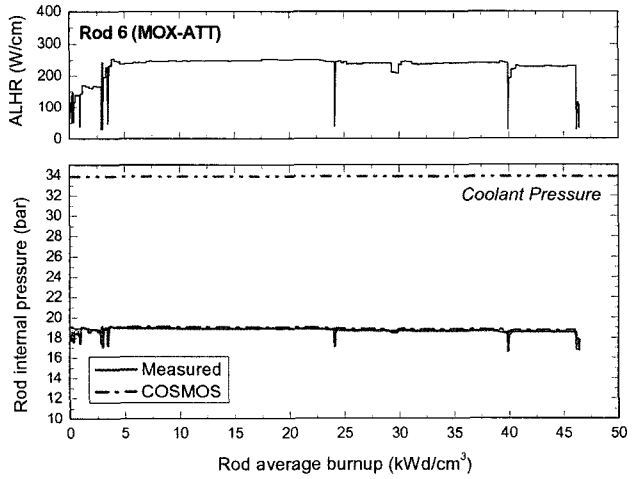

(b)

Fig. 11 . Comparison of the COSMOS Calculated Rod Internal Pressure with the Measured Value for (a) Rod 3 and (b) Rod 6

The measured fuel temperature during the steady-state irradiation was compared with the value predicted by the COSMOS code. The measured temperatures in Rod 3 and Rod 6 show good agreement with the predicted values within the measurement error as shown in Fig. 10.

Fig. 10 also displays the fission gas release threshold temperature with the assumption that the threshold temperature of the MOX fuel is similar to that of UO_2 fuel. There seems not to be any significant fission gas release in both fuel rods during the first cycle since the fuel temperature was lower than the threshold value for fission gas release.

The rods were initially filled with 10 bar helium at room temperature. The rod internal pressure was measured on-line during the in-pile test. The change in rod internal pressure reflects the degree of fission gas release and the change of free volume influenced by both fuel densification /swelling and cladding creep-down. Since the fuel temperature was lower than the threshold value during the first cycle, the rod internal pressure for both rods can be influenced only by the fuel and cladding geometrical change.

The measured rod internal pressure was compared with the COSMOS code prediction in Fig. 11. The rod internal pressure of ~20 bar for Rod 3 and ~19 bar for Rod 6 was measured during steady-state operation. Considering the fact that both rods were filled with 10 bar helium and that the Rod 6 was irradiated at higher power than Rod 3, the lower measured pressure of Rod 6 than that of the Rod 3 might be a little out of expectation. This reversed pressure can be explained by the larger densification in Rod 6 than in Rod 3 and the more dominant densification effect on the pressure than the effect of rod power in this case. The measured rod internal pressure agreed well with the COSMOS code prediction for both rods.

5. CONCLUSIONS

The main results from the first cycle of irradiation of the IFA-651 and the analysis of the measured data with COSMOS code have been presented and some basic conclusions are as follows:

(1) IFA-651 has been successfully irradiated for the first cycle. All rod instrumentation has functioned satisfactorily.
(2) Based on the rig power calibrations, the HELIOS calculation results can be applied with small adjustment to determine the rig and rod power.
(3) The MOX fuel shows more stable in-pile behavior than IMF fuel taking into account the thermal and rod internal pressure behaviors.
(4) Both the on-line measured performance data and the COSMOS code predictions agreed well for the transient fuel temperature, steady state fuel temperature and the rod internal pressure

Acknowledgements

The authors would like to express their appreciation to

Mr. G. Rossiter (BNFL) and Dr. Ch. Hellwig (PSI) for their contribution to the in-pile test of IFA-651.

REFERENCES

[1] Yang-Hyun Koo, Byung-Ho Lee and Dong-Seong Sohn, "COSMOS: A computer code for the analysis of LWR UO_2 and MOX fuel rod," Journal of the Korean Nuclear Society, **30**, 541 (1998).
[2] Y W Lee, H S Kim, S H Kim, C Y Joung, S H Na, G Lederger, P Heimgartner, M Pouchon & M Burghartz, "Preparation of Simulated Inert Matrix Fuel with Different Powders by Dry Milling Method", J. of Nucl. Mater., **274**, 7 (1999).
[3] R Stephen, "SBR MOX Fuel Manufacture", Halden Project Workshop on Fabrication, Performance and Modelling of MOX Fuel, Halden, 28-29 September 1999.
[4] H.Kampf and G.Karsten, Nucl. Tech., 9, 288 (1970).
[5] Byung-Ho Lee, Yang-Hyun Koo, Jin-Sik Cheon, Je-Yong Oh and Dong-Seong Sohn, "A Unified Thermal Conductivity Model for LWR MOX Fuel Considering Its Microstructural Characteristics", Actinide-2001, Japan.
[6] W.Wiesenack, T.Tverberg, "Thermal performance of high burnup fuel- in-pile temperature data and analysis", 2000 International Topical Meeting on LWR Fuel Performance, Park City, Utah, April 10-13, 2000.
[7] D. Baron, Proc. of Seminar on Thermal Performance of High Burn-up LWR Fuel, France, p.99 (1998).
[8] Y.Philipponneau, J. Nucl. Maters., **188**, 194 (1992).
[9] M. Lippens and the COMETHE team, Proc. of the Seminar on Thermal Performance of High Burn-up LWR fuel, NEA, France, (1998).
[10] C.T.Walker, et al., J. Nucl. Maters., **245**, 169 (1997).
[11] G.A.Gates, et al., Proc. of Seminar on Thermal Performance of High Burn-up LWR Fuel, France, p.301 (1998).
[12] L.Heins, H.Landskron, Int. Symposium on MOX Fuel Cycle Technologies for Medium and Long-term Deployment, IAEA-SM-358/21, Austria (1999).
[13] M.Lippens, et al., Proc. of the Seminar on Thermal Performance of High Burnup LWR Fuel, France, p.243 (1998).
[14] Yang-Hyun Koo, Byung-Ho Lee, Jin-Sik Cheon, and Dong-Seong Sohn, "Modeling and parametric studies of the effect of inhomogeneity on fission gas release in LWR MOX fuel," Annals of Nuclear Energy, **29**, 271 (2002).
[15] Byung-Ho Lee, Yang-Hyun Koo and Dong-Seong Sohn, "Void effect combined with water chemistry on corrosion behavior of Zircaloy-4 cladding in PWR", International Topical Meeting on LWR Fuel Performance, Park City, USA, 2000.
[16] Byung-Ho Lee, Yang-Hyun Koo, Jin-Sik Cheon and Dong-Seong Sohn, "Modeling of creep behavior of Zicraloy-4 by considering metallurgical effect", Annals of Nuclear Energy, **29**, 1 (2002).